© EARSeL and Warsaw University, Warsaw 2005. *Proceedings of 4th EARSeL Workshop on Imaging Spectroscopy. New quality in environmental studies*. Zagajewski B., Sobczak M., Wrzesień M., (eds)

THE POTENTIAL OF THE PROPOSED CANADIAN HERO MISSION FOR GEOSCIENCE APPLICATIONS

Karl Staenz[1], Robert A. Neville[1], Robert Hitchcock[2], Patrick Assouad[3], Khalid Omari[1], Lixin Sun[4], Martin Bergeron[5], and H. Peter White[1]

1. Canada Centre for Remote Sensing, Natural Resources Canada, 588 Booth Street, Ottawa, Ontario, Canada K1A 0Y7; karl.staenz@ccrs.nrcan.gc.ca
2. Prologic Systems Ltd., 75 Albert Street, Suite 206, Ottawa, Ontario, Canada
3. ACG Space Technologies Corp., 202-119 Clarence Street, Ottawa, Ontario, Canada K1N 5P5
4. Dendron Resources Surveys Inc., Lady Ellen Place, Ottawa, Ontario, Canada K1Z 5L9
5. Canadian Space Agency, 6767 Route de l'Aéroport, St. Hubert, Quebec, Canada J3Y 8Y9

ABSTRACT

With the development of the conceptual design of the Canadian Hyperspectral Environment and Resource Observer (HERO) mission, its performance needs to be evaluated for different applications areas. Accordingly, this paper investigated the potential of the HERO mission for geoscience applications, such as mineral identification for mapping, exploration and monitoring mine tailings. Hyperspectral data were simulated to match the HERO characteristics, using as input fraction maps derived from airborne data and high-resolution library spectra to represent the endmembers of the different materials. Noise and various sensor-related artifacts were added to match the expected HERO characteristics. The original data and the simulated data were processed the same way, applying a MODTRAN 4.2 based atmospheric correction prior to spectral linear unmixing to produce mineral abundance maps. The results indicate the original data and HERO simulated data products are generally similar. However, significant differences occur for the smaller fractions.

INTRODUCTION

The Canada Centre for Remote Sensing (CCRS) has been involved in research to develop and improve hyperspectral technologies for geoscience applications, such as mine site monitoring and assessment (revegetation, acid mine drainage, and environmental impact of mine activities on the surroundings), mineral identification and lithological mapping. Airborne hyperspectral imagery, acquired over a mining area near Cuprite (Nevada, U.S.A.) and mine tailings area near Sudbury (Ontario, Canada), has been used successfully to produce different information products, such as baseline maps of abandoned mine sites, revegetation maps, acidity maps, mineral and rock unit maps (i), (ii), (iii), (iv), (v)). Image data were classified through the use of spectral unmixing techniques, which can separate target types based on unique absorption features in the visible and near infrared (VNIR) and short-wave infrared (SWIR) portions of the electromagnetic spectrum. This information can be used to map vegetation and tailings extent, diagnose vegetation health, separate differentiate mineral compounds resulting from various stages of sulphide oxidation, and identify and map minerals.

The long term monitoring of mine sites and their surroundings, and geological mapping of vast remote areas, such as the Canadian Arctic, can only be achieved on an operational basis with spaceborne systems. With the first hyperspectral systems, NASA's Hyperion and ESA's CHRIS in space, CCRS' activities are focusing more and more on the use of satellite data. These systems are technology demonstrators and as such do not provide sufficient data quality, coverage and revisit frequency for operational usage. Operational spaceborne systems such as the proposed Canadian Hyperspectral Environment and Resource Observer (HERO) mission are needed (vi).

In order to evaluate the potential of the HERO mission for geoscience applications, HERO data were simulated from airborne hyperspectral data and library spectra. Information products investigated were similar to the ones retrieved from airborne data as mentioned above. The simulated

data were processed in the same way as the original data and compared quantitatively against each other. Major processing steps include the removal of atmospheric effects, and application of linear spectral unmixing. These processing steps were carried out using the Imaging Spectrometer Data Analysis System (ISDAS:vii) developed at the Canada Centre for Remote Sensing (CCRS).

HERO

The Canadian Space Agency (CSA), CCRS and industry are currently developing a hyperspectral spaceborne mission. The mission is currently in its conceptual stage (phase A) to define different mission and instrument scenarios taking into account the established user requirements. The mission will consist of the space, ground, and applications segments. The space segment consists of the payload (imager), the platform, and the launcher. The imager will operate in 10 nm wide bands in the VNIR and SWIR portions of the electromagnetic spectrum. The ground sampling distance will be 30 m. The minimum requirements for the peak signal-to-noise (SNR) are 550: 1 in the VNIR (430 – 1000 nm) and 200:1 in the SWIR II (2000 – 2450 nm) for a 30% reflectance target viewed under a 30° solar zenith angle. The baseline instrument characteristics, which are based on the user requirements, are summarized in Table 1.

Table 1: HERO sensor characteristics (FWHM = full width half maximum; SNR for 30% reflectance target and 30° solar zenith angle).

Altitude	705 km
Swath Width	36 km
Ground Sampling Distance (GSD)	30 m
Keystone	≤ 0.1 x GSD
Spectral Coverage	430 – 2450 nm
Spectral Resolution (FWHM)	~10 nm
Spectral Sampling Interval (SSI)	~10 nm
Number of Bands	240 (60 VNIR + 180 SWIR)
Smile/frown	≤ 0.1 x SSI
Peak Signal-to-Noise (SNR) - VNIR (430 – 1000 nm) - SWIR I (1000 – 2000 nm) - SWIR II (2000 – 2450 nm)	 ≥ 550:1 ≥ 320:1 ≥ 200:1
Photo Response Non-Uniformity (residual)	≤ 0.1%
Dark Current Non-Uniformity (residual)	≤ 1 %
Roll Angle across track	≤ 20°
Re-Look Time	7 days
Equator Crossing Time	11:00

The functional elements of the ground segment include: mission control, satellite and payload control, data reception, quick-look facility, data processing (including calibration, atmospheric correction, etc.), data archiving, generation of data products, distribution of data and/or data products to users, and order request functions.

The development of data preprocessing and information extraction algorithms and products is part of the application segment.

DATA SIMULATION

A two-step simulation process was used to generate the HERO simulated data representing the Cuprite mineral area and Sudbury mine tailings areas. In a first step, a basic (original) data cube was produced. In a second step, the simulated data cube was generated to match the HERO baseline characteristics as shown in Table 1 using the original cube as input.

ORIGINAL DATA GENERATION

Cuprite Data: In a first step, 20-m Airborne Visible/Infrared Imaging Spectrometer (AVIRIS) data (viii), acquired on June 12, 1996 over a mineral area near Cuprite, Nevada (U.S.A.) was used to select endmembers with an automatic endmember technique, namely the Iterative Error Analysis (IEA;ix). A total of 10 pure and 4 mixed endmembers and 1 dark endmember representing shadow were selected as shown in Table 2. The AVIRIS scene was then unmixed with a constrained linear procedure (x) to generate the fraction maps for each of the selected endmembers. USGS library (xi) and PIMA (xii) spectra were used to represent the endmembers extracted from the AVIRIS data in order to maximize the spectral sampling and resolution. For this purpose, the USGS reflectance spectra (351 nm to 1300 nm) and the PIMA reflectance spectra (1300 nm to 2500 nm) were concatenated to form the endmember spectra. The combined USGS and PIMA spectra were then used as the endmembers to reconstruct the Cuprite reflectance cube via linear mixing, using the original AVIRIS fraction maps as a basis for the mixing. These steps generated spectrally high-resolution data, which were better suited to simulate the HERO characteristics than the AVIRIS data.

Sudbury Data: 5-m airborne hyperspectral data acquired with Probe-1 (xiii) on July 8, 1999 over the Copper Cliff mine tailings site in Sudbury, Ontario (Canada) together with ground-based ASD spectra (xiv) from the SpecMin library (xii) were used to generate the initial data cube. For this purpose, the Probe-1 reflectance scene was unmixed with a constrained linear procedure to generate the fraction maps for each of the 17 selected endmembers, which were selected from the USGS library (xi) due to the lack of pure pixels in the scene. These endmembers, listed in Table 2, were then replaced with ASD spectra, which were convolved to a 10-nm full width at half maximum (FWHM) bandwidth using a Gaussian bandpass profile and resampled to a 5-nm interval to form a new set of endmembers. Subsequently, these spectra were used to reconstruct a new cube via linear mixing, using the original Probe-1 fraction maps as a basis for the mixing.

In a last step, these reflectance cubes were transferred to HERO at-sensor radiance using the ISDAS atmospheric correction tool (xv). The overpass times, dates, and RT code input parameters used in the simulations are summarized in Table 3.

HERO Data Simulation

The generated original data cubes (Cuprite, Sudbury) were processed according to Figure 1 to simulate the HERO baseline (Table 1). During the simulation, the original image was replicated to fill the full HERO swath of 36 km. Noise included the following terms: scene shot, dark shot, self emission shot, readout electronics, and photo response and dark signal non-uniformity. All terms, except the photo response and dark signal non-uniformities were assumed to follow Gaussian statistics.

DATA PROCESSING

In order to quantitatively assess the information products, the original data were spectrally and spatially adapted to the HERO characteristics and processed the same way as the simulated cubes. In addition, the simulated cubes were intentionally not corrected for senor artifacts to evaluate the full impact of the simulation process. It is clear that the usual way to process data is to remove the artifacts prior to information extraction.

Original Data

The original reflectance data were spectrally convolved to the HERO characteristics. Endmembers as listed in Table 2 were then extracted from the 20-m Cuprite data cube and, subsequently, weakly constrained liner unmixing was applied (x). The resulting fraction maps were then resampled to 30 m using a bi-linear transformation.

For the 5-m Sudbury data, the library (ASD) endmembers (Table 2) were used as input into the fully constrained linear unmixing ISDAS procedure to produce the fraction maps, which were averaged to 30 m.

These cubes are referred to in the following text as reference cubes.

Table 2: Endmembers selected for the generation of the simulated HERO cubes.

Endmember #	Cuprite Data Mineral	Sudbury Data Mineral
1	Alunite	Calcite
2	Buddingtonite	Chlorite
3	Calcite	Dolomite
4	Dickite	Ferrihydrite
5	Gypsum	Water
6	Kaolinite	Goethite
7	Montmorillonite	Gypsum
8	Muscovite	Hematite
9	Opal	Illite
10	Varnish	Jarosite
11	Alunite/Dickite Mixture (90%/10%)	Maghemite
12	Alunite/Dickite Mixture (70%/30%)	Magnetite
13	Alunite/DickiteMixture (50%/50%)	Melantorite
14	Alunite/Kaolinite Mixture (40%/60%)	Pyrite
15	Dark (zeroes)	Pyrrhotite
16	-	Quartz
17	-	Vegetation

Table 3: Input parameters for MODTRAN4.2 code runs.

Parameter	Cuprite Data	Sudbury Data
Atmospheric model	mid-latitude summer	mid-latitude summer
Aerosol model	Continental (rural)	continental (rural)
Date of overflight	May 1	July 14
Time of day (GMT)	18:20	14:15
Solar zenith angle	31.05°	48.94°
Solar azimuth angle	129.73°	132.43°
Sensor zenith angle	variable	variable
Sensor azimuth angle	variable	variable
Tilt angle across swath	0°	0°
Terrain elevation (above sea level)	1.524 km	0.300 km
Sensor altitude (above sea level)	640 km	640 km
Water vapour content	1.25 g/cm2	1.25 g/cm2
Ozone column	as per model	as per model
CO2 mixing ratio	as per model	as per model
Horizontal visibility	23 km	23 km
Wavelength grid interval	1 cm-1	1 cm-1

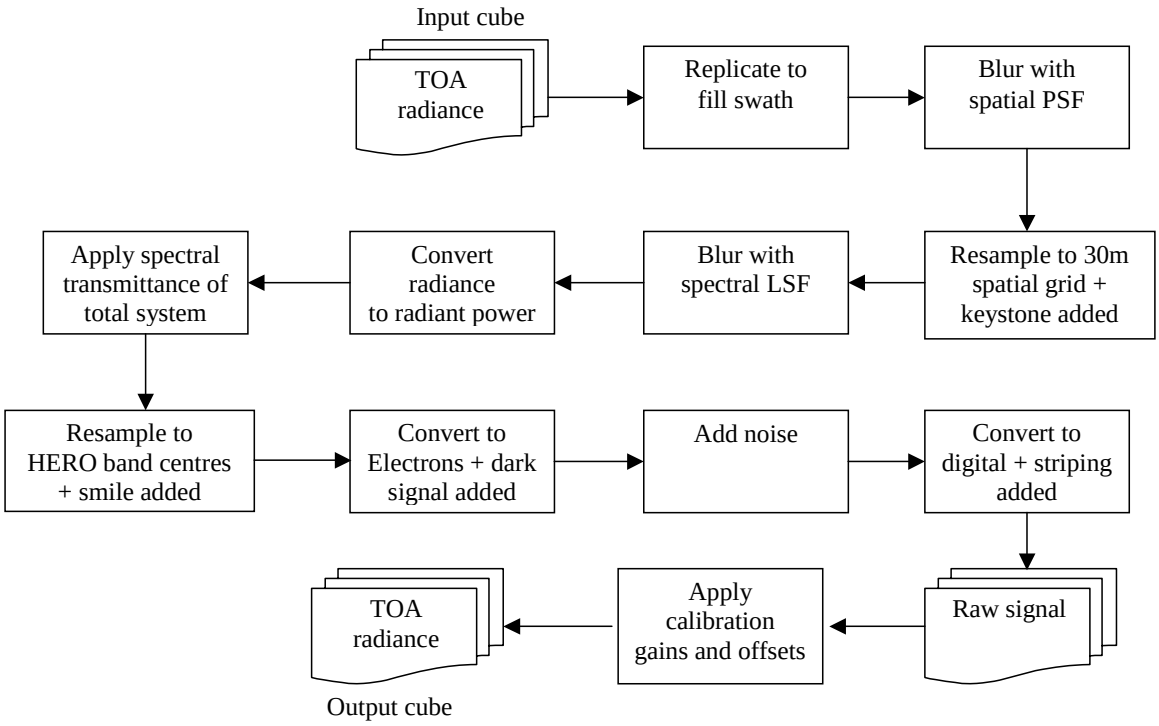

Figure 1: Processing scheme for the HERO baseline simulation (TOA = Top Of Atmosphere, PSF = Point Spread Function. LSF = Line Speread Function).

Simulated Data

In a first step, an atmospheric correction was performed to convert the at-sensor radiance of the HERO simulated data to reflectance using the same procedure as mentioned in section “Original Data Generation”. MODTRAN4.2 input parameters for the Cuprite and Sudbury cubes were the same as listed in Table 2. The processing steps as listed in section “Original Data” were repeated for the two different cubes.

Comparison

The changes of the fractions retrieved from the reference and simulated cubes were calculated using different measures. The Root Mean Square Error (RMSE) was calculated as an overall measure defined as follows:

$$RMSE = \sqrt{\frac{1}{n_x n_y}\sum_{x=1}^{n_x}\sum_{y=1}^{n_y}\left[f_R(x,y) - f_S(x,y)\right]^2}, \quad (1)$$

where f_S is the fraction from the simulated SNR cubes, f_R is the fraction from the reference cube, n_x is total number of pixels in a line, n_y is the number of lines in the cube, and x and y are the pixel and line position, respectively.

The absolute error (AE) was used as a fidelity measure of the spatial variations between the reference and simulated data. AE is defined as follows:

$$AE = f_s(x,y) - f_r(x,y) \quad (2)$$

In addition, a comparison of the retrieved endmembers (Cuprite data), extracted from the reference and simulated data, was carried out using the average relative error (ARE) and Spectral Angle Mapper (SAM) (xvi). These measures can be written as:

$$ARE = \frac{1}{n_b} \sum_{b=1}^{n_b} 100 \frac{\sqrt{(em_R(b) - em_S(b))^2}}{em_R(b)} \tag{3}$$

and

$$SAM = \cos^{-1}\left(\frac{\sum_{b=1}^{n_b} em_R(b)\ em_S(b)}{\sqrt{\sum_{b=1}^{n_b} [em_R(b)]^2 \sum_{b=1}^{n_b} [em_S(b)]^2}} \right), \tag{4}$$

where $em_r(b)$ is the endmember reflectance in band b of the reference cube and $em_s(b)$ is the endmember reflectance in band b of the simulated cube. SAM varies between 0 and $\Pi/2$ where 0 indicates a perfect match between reference and simulated endmember spectra. While ARE provides a measure of the overall difference between reference and simulated endmember spectra, SAM, which is insensitive to gain factors, gives a good indication about the preservation of absorption features in the simulated data.

RESULTS

Endmembers

Endmembers extracted from the reference and simulated Cuprite data cube are compared against each other as well as with the original endmembers (Table 4). All the pure endmembers were extracted from the simulated cube, although the automatic IEA procedure selected some of the endmembers in a different order, resulting in a different endmember number for a given endmember. The mixture endmembers as used to generate the original data cube were not retrieved since they are represented by a linear combination of the pure endmembers. (The IEA uses linear unmixing to detect the endmembers.)

Differences between endmember reflectance spectra, extracted from reference data and simulated data, generally revealed a satisfactory match. The relatively low SAM values indicate that the typical shapes of the mineral absorption features were preserved in the simulated data. Even for gypsum with a value of 0.069, the distinct feature around 2210 nm is preserved well. However, there are amplitude differences between the endmembers retrieved from the reference and simulated data of up to 9 % ARE. It should be noted in this context that endmember spectra, extracted from the reference data and simulated data, are not necessarily derived from the same pixels, thereby enhancing the probability of spectral differences for a specific endmember. In addition, some of these differences were introduced in the simulation process (Figure 1) and, subsequently, in the atmospheric correction procedure. The latter enhances errors especially in the atmospheric absorption features mainly due to noise and spectral artifacts (smile, shifts). In these regions errors of up to 32 % occur for gypsum. In order to further illustrate these statements, an example of the endmember spectra of alunite is shown in Figure 2. A comparison of the dark endmember revealed significant errors. This was expected, and is due to the noise added in the simulation process, which has a larger impact on the low signal than on the other endmembers.

The same set of library endmembers were used to unmix both Sudbury data cubes and, therefore, there is no analogous endmember analysis.

Table 4: Endmembers retrieved from the Cuprite data cube.

Original 15 Endmembers used to generate cube		Reference Cube	HERO Simulated Cube	Spectral Angle Mapper (SAM)	Average Relative Error (ARE)
em#	mineral	em#	em#		%
1	alunite	5	3	0.019	3.76
2	buddingtonite	10	12	0.027	2.72
3	calcite	9	8	0.023	7.22
4	dickite	7	7	0.022	3.89
5	gypsum	3	6	0.069	8.83
6	kaolinite	11	14	0.022	4.22
7	montmorillonite	8	11	0.019	2.91
8	muscovite	6	5	0.029	2.12
9	opal	1	1	0.022	3.69
10	desert varnish	4	4	0.031	3.04
11	alunite/dickite 90/10				
12	alunite/dickite 70/30				
13	alunite/dickite 50/50				
14	alunite/kaolinite 40/60				
15	dark (zero) spectra	2	2	0.221	62.06

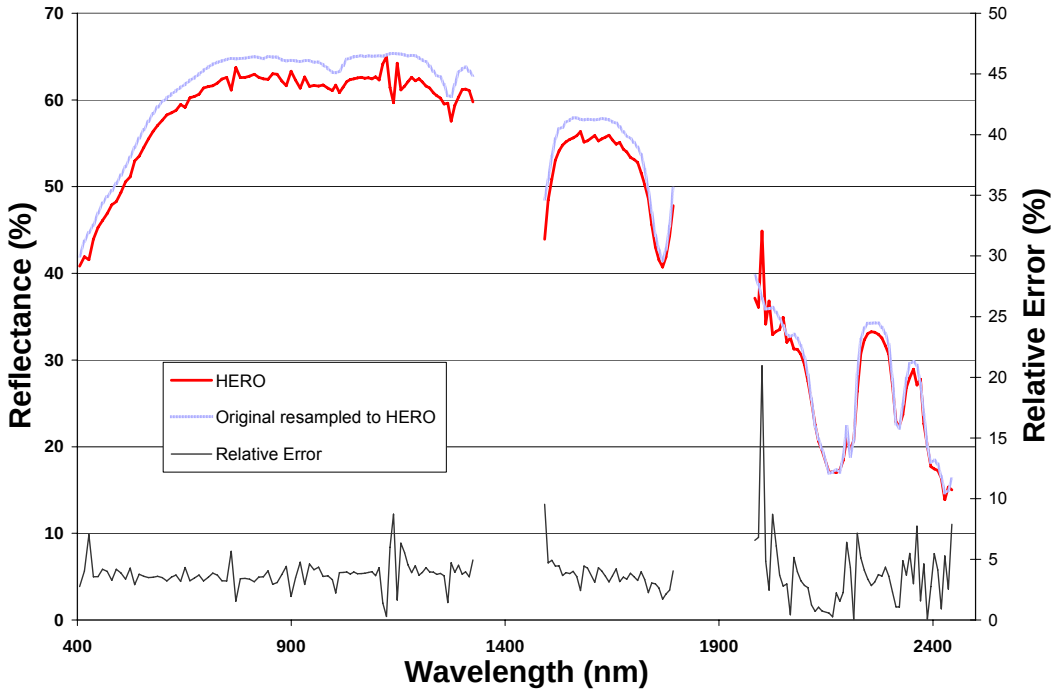

Figure 2: Relative Error between Endmember spectra of alunite extracted from the reference and simulated data cubes.

OVERALL FRACTION ERRORS

The RMSE, calculated with equation (1), between the fractions extracted from the reference and the simulated cubes are shown in Figure 3 for the Cuprite and Sudbury cubes for the endmembers listed in Table 2. Most RMSE values are below 0.06 with the exception of Sudbury water, vegetation and pyrrhotite endmembers which had RMSE values larger than 0.08.

SPATIAL ERROR DISTRIBUTION

A similar trend as shown for the RMSE was revealed by the fraction differences between the reference and the simulated cubes measured by the AE (equation 2). As an example, Figure 4 shows the frequency distribution of AE, calculated for each pixel of the fraction (abundance) map of endmembers alunite (Cuprite cube) and pyrrhotite (Sudbury cube). Both graphs show a similar trend, although larger errors occur for pyrrhotite. The AE of most pixels in the alunite fraction maps are below 0.1 and only about 1 % of the pixels have larger errors of up to 0.4. Most pixels indicate similar fractions for the Sudbury cube. About 9 % of the pixels show significant fraction differences of up to 0.8 for pyrrhotite. With mean fractions of 0.093 (alunite) and 0.040 (pyrrhotite) extracted from the reference data these absolute errors translate to very large relative errors. This is due to the small fractions extracted for the tailings composition materials. Even a relatively small fraction difference between the reference and simulated cubes can result in a relative error of several tens of percent. It should be noted that the zero-fractions were not included in the mean calculations. Similar results were observed for the other endmember fraction maps of the two data sets with up to 3 % (Cuprite) and 2 % (Sudbury) of pixels showing an AE of over 0.1, respectively; at the same time the relative errors exceeded those for the Cuprite data.

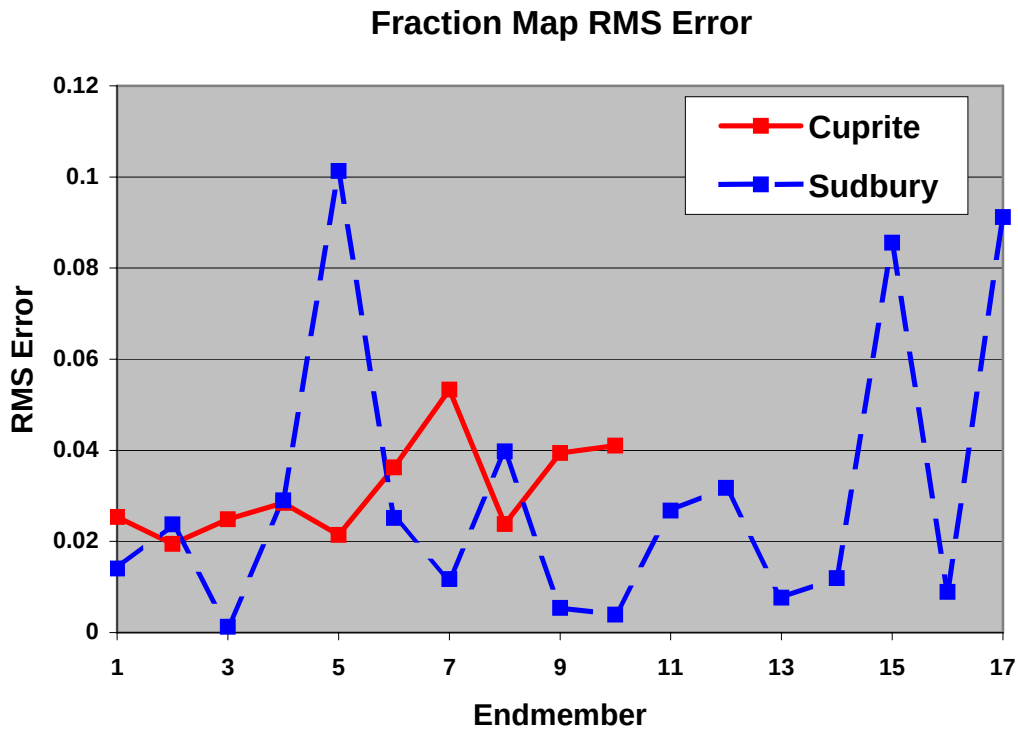

Figure 3: RMSE of the fractions extracted from the reference and simulated data cubes for the different endmembers as listed in Table 2.

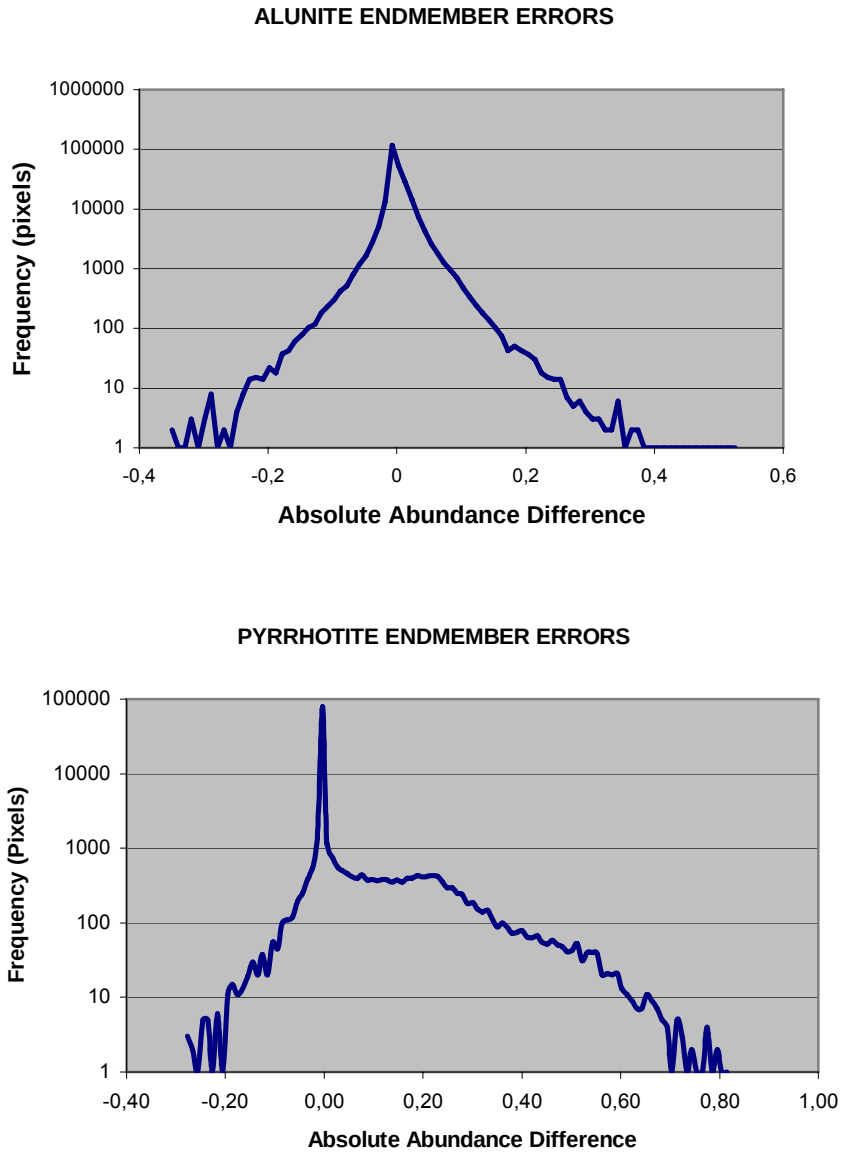

Figure 4: Frequency (pixel) distribution of the absolute error (AE) for endmember alunite (Cuprite cube) and pyrrhotite (Sudbury cube).

CONCLUSIONS

The potential of HERO for identification and mapping of minerals in the exploration and mine tailings monitoring context was investigated in this study. For this purpose, simulated HERO data cubes were generated from fraction maps derived from airborne data of the Cuprite mining district and Sudbury mine tailings areas and library spectra using linear spectral mixture analysis. In general, the errors between reference and simulated data products are relatively low except for cases of low endmember fraction where relative errors of over 100% occur. All of the 10 mineral endmembers, retrieved from the Cuprite reference data, could also be extracted from the simulated data. In the case of the Sudbury data cube, the same set of library spectra were used for unmixing purposes eliminating the extraction of scene-based endmembers. It is expected that the agreement between the two sets of results can be improved if corrections are made for sensor artifacts, such as striping and smile, which were introduced in the simulation process. This would be part of the normal preprocessing procedure to be applied to any data prior to information extraction. Based on these results, derived from data uncorrected for sensor artifacts, HERO has the potential

to deliver high quality data products, capable of supporting mineral exploration activities, monitoring mine tailings sites, and very likely a large number of other applications for which airborne hyperspectral data have been successfully used.

ACKNOWLEDGEMENT

The authors acknowledge the financial contribution of the Canadian Space Agency for the study presented in this paper.

REFERENCES

i Staenz, K., R.A. Neville, J. Lévesque, T. Szeredi, V. Singhroy, G.A. Borstad, and P. Hauff, 1999. Evaluation of casi and SFSI Hyperspectral Data for Environmental and Geological Applications – Two Case Studies. Canadian Journal of Remote Sensing, 25(3): 311- 322.

ii Lévesque, J., K. Staenz, J. Shang, R.A. Neville, P. Yearwood, and V. Singhroy, 1999. Temporal Monitoring of Mine Tailings Revegetation Using Hyperspectral Data, Sudbury, Ontario. In: Proceedings of the Thirteenth Int. Conference on Applied Geologic Remote Sensing, Vancouver, British Columbia, Canada, Vol. 2, 21-28.

iii Neville, R.A., J. Lévesque, K. Staenz, T. Szeredi, C. Nadeau, P. Hauff, and G. Borstad, 2003. Hyperspectral Imagery for Mineral Exploration: Comparison of Data from two Airborne Sensors. Canadian Journal of Remote Sensing, 29(1): 99-110.

iv Richter, N., H. Kaufmann, and K. Staenz, 2004. Hyperspectral TRWIS III Data to Delineate the Kam Kotia Mine Tailings Areas (Ontario, Canada). In: Remote Sensing for Environmental Monitoring, GIS Applications, and Geology IV, edited by Ehlers, M., Posa, F., Kaufmann, H.J., Michel, U., De Carolis, G., Proceedings of SPIE 5574: 214-223.

v Truong, Q.S. Bob, G.A. Borstad, K. Staenz, R. Neville, R. Leslie, P. Riggs, and V. Bragin, 2003. Multispectral and Hyperspectral Imagery for Safeguards and Verification of Remote Uranium Mines. In: Proceedings of the 44th Annual Meeting of the Institute of Nuclear Materials Management (INMM), Phoenix, Arizona, CD-ROM (7 pages).

vi Staenz, K., and A.H. Hollinger, 2003. A Canadian Hyperspectral Spaceborne Mission – Applications and User Requirements. In: 3rd EARSeL Workshop on Imaging Spectroscopy, edited by M. Habermeyer, A. Mueller, & S. Holzwarth (EARSeL, Paris), 31-35.

vii Staenz, K., T. Szeredi, and J. Schwarz, 1998. ISDAS - A System for Processing/Analyzing Hyperspectral Data. Canadian Journal of Remote Sensing, 24(2): 99-113.

viii Green, R. O., M.L. Eastwood, C.M. Sarture, T.G. Chrien, M. Aronsson, B.J. Chippendal, J.A. Faust, B.E. Pavri, C.J., Chovit, M. Solis, M.R. Olah, and O. Williams, 1998. Imaging Spectroscopy and the Airborne Imaging Visible/Infrared Imaging Spectrometer (AVIRIS). Remote Sensing of Environment, 65: 227-248.

ix Neville, R.A., K. Staenz, T. Szeredi, J. Lefebvre, and P. Hauff, 1999. Automatic Endmember Extraction from Hyperspectral Data for Mineral Exploration. In: Proceedings of the Fourth International Airborne Remote Sensing Conference and Exhibition / 21st Canadian Symposium on Remote Sensing, Ottawa, Ontario, Canada, Vol. 2: 891-896.

x Shang, J., R.A. Neville, K. Staenz, L. Sun, B. Morris, P. Howarth, 2004. A Comparison of Fully Constrained and Weakly Constrained Unmixing through Mine-Tailing Composition Mapping. Submitted to Canadian Journal of Remote Sensing.

xi USGS, 2002. USGS Digital Spectral Library, Denver, Colorado, U.S.A. http://speclab.cr.usgs.gov/spectral-lib.html.

xii SpecMin, 2002. How to Use SpecMinTM, Pro Version 3.1. Spectral International Inc., Arvada, Colorado, U.S.A., 38 pages.

xiii ESSI, 2001. About Probe-1, Kalispell, MT, U.S.A., www.erthsearch.com/technology.

xiv Analytical Spectral Devices Inc., 1997. FieldSpecTM User's Guide, Analytical Spectral Devices Inc., Boulder, CO, U.S.A., 81 pages.

xv Staenz, K., and D. Williams, 1997. Retrieval of Surface Reflectance From Hyperspectral Data Using a Look-Up Table Approach. Canadian Journal of Remote Sensing, 23(4): 354-368.

xvi Kruse, F.A., A.B. Lefkoff, and J.B. Dietz, 1993. Expert System-Based Mineral Mapping in Northern Nevada Death Valley, California/Nevada, Using the Airborne Visible/Infrared Imaging Spectrometer (AVIRIS). Remote Sensing of Environment, 44: 309-336.